European Journal of Mineralogy

Hydroxyferroroméite, a new secondary weathering mineral from Oms, France

--Manuscript Draft--

Manuscript Number:	
Article Type:	Research paper
Full Title:	Hydroxyferroroméite, a new secondary weathering mineral from Oms, France
Short Title:	Hydroxyferroroméite from Oms, France
Corresponding Author:	Stuart J Mills Museum Victoria AUSTRALIA
Corresponding Author E-Mail:	SMills@museum.vic.gov.au
Order of Authors:	Stuart J Mills
	Andrew Christy
	Mike Rumsey
	John Spratt
	Erica Bittarello
	Georges Favreau
	Marco Ciriotti
	Christian Berbain
Abstract:	Hydroxyferroroméite, ideally (Fe2+1.5□0.5)Sb5+2O6(OH), is a new secondary mineral from the Correc d'en Llinassos, Oms, Pyrénées-Orientales Department, France. Hydroxyferroroméite occurs as yellow to yellow-brown powdery boxwork replacements up to about 50 μm across after tetrahedrite in a siderite–quartz matrix. No distinct crystals have been observed. The empirical formula (based on 7 (O + OH) pfu) is: (Fe2+1.07Cu2+0.50 Zn0.03Sr0.03Ca0.01□0.36)Σ2(Sb5+1.88Si0.09Al0.02As0.01)Σ2O6((OH)0.86O0.14). X-ray photoelectron spectroscopy was used to determine the valence states of Sb, Fe and Cu. Hydroxyferroroméite crystallises in the space group Fd-3m, with the pyrochlore structure and has the unit cell parameters: a = 10.251(31) Å, V = 1077(6) Å3 and Z = 8. A model, based on bond valence theory, for incorporation of Fe2+ into A site of the pyrochlore structure is proposed.
Keywords:	Hydroxyferroroméite; pyrochlore; roméite; X-ray photoelectron spectroscopy; antimonate.
Manuscript Region of Origin:	FRANCE
Requested Editor:	Sergey V. Krivovichev
Suggested Reviewers:	daniel atencio Universidade de Sao Paulo datencio@usp.br
	ulf halenius natural history museum sweden Ulf.Halenius@nrm.se
Opposed Reviewers:	
Additional Information:	
Question	**Response**
Author Comments:	We would like to request colour fees be waived because Andy is an AE.

Hydroxyferroroméite, a new secondary weathering mineral from Oms, France

Stuart J. Mills[1,*], Andrew G. Christy[2], Mike S. Rumsey[3], John Spratt[4], Erica Bittarello[5], Georges Favreau[6], Marco E. Ciriotti[7] & Christian Berbain[8]

[1]Geosciences, Museum Victoria, GPO Box 666, Melbourne 3001, Victoria, Australia

[2]Department of Applied Mathematics (Research School of Physics & Engineering) and Research School of Earth Sciences, Mills Rd, Australian National University, Canberra, ACT 2601, Australia

[3]Department of Earth Sciences, Natural History Museum, Cromwell Road, London SW7 5BD, United Kingdom

[4]Department of Facilities, Natural History Museum, Cromwell Road, London SW7 5BD, United Kingdom

[5]Dipartimento di Scienze della Terra, Università degli Studi di Torino, via Tommaso Valperga Caluso 35, I-10125 Torino, Italy

[6]421 avenue Jean Monnet, 13090 Aix-en-Provence, France

[7]Associazione Micromineralogica Italiana, via San Pietro 55, I-10073 Devesi-Cirié, Torino, Italy

[8]32 rue R. Cassin, 66270 Le Soler, Pyrénées-Orientales, France

*Email: smills@museum.vic.gov.au

Abstract

Hydroxyferroroméite, ideally $(Fe^{2+}_{1.5}\square_{0.5})Sb^{5+}_{2}O_6(OH)$, is a new secondary mineral from the Correc d'en Llinassos, Oms, Pyrénées-Orientales Department, France. Hydroxyferroroméite occurs as yellow to yellow-brown powdery boxwork replacements up to about 50 μm across after tetrahedrite in a siderite–quartz matrix. No distinct crystals have been observed. The empirical formula (based on 7 (O + OH) *pfu*) is: $(Fe^{2+}_{1.07}Cu^{2+}_{0.50}Zn_{0.03}Sr_{0.03}Ca_{0.01}\square_{0.36})_{\Sigma 2}(Sb^{5+}_{1.88}Si_{0.09}Al_{0.02}As_{0.01})_{\Sigma 2}O_6((OH)_{0.86}O_{0.14})$. X-ray photoelectron spectroscopy was used to determine the valence states of Sb, Fe and Cu. Hydroxyferroroméite crystallises in the space group *Fd*-3*m*, with the pyrochlore structure and has the unit cell parameters: a = 10.251(31) Å, V = 1077(6) Å^3 and Z = 8. A model, based on bond valence theory, for incorporation of Fe^{2+} into *A* site of the pyrochlore structure is proposed.

Keywords: Hydroxyferroroméite, pyrochlore, roméite, X-ray photoelectron spectroscopy, antimonate.

1. Introduction

In the framework of a general search for unusual secondary minerals in France, the small Oms deposit caught the attention of two of the authors (GF + CB) due to the relative abundance of ullmannite, occurring in a weathered environment. The first search for Ni secondary minerals yielded the first French occurrence of bottinoite and a bright yellow mineral which turned out to be a new species, omsite (Berbain & Favreau, 2007; Mills *et al.*, 2012). While trying to get deeper knowledge of the secondary minerals at Oms, a mineral looking like "bindheimite" was collected. As it was found in a zone devoid of lead, an EDS

analysis was carried out at the Association Jean Wyart, Paris, which showed a unique combination of elements suggesting another new species.

The mineral and name (IMA2016–006) were approved by the IMA–CNMNC prior to publication. The mineral is named according to the nomenclature of the pyrochlore supergroup (Atencio *et al*., 2010; Christy & Atencio, 2013). Its end-member formula is characterized by OH^- dominance at the *Y* site, Fe^{2+} at the *A* site and Sb^{5+} dominance at the *B* site. The type specimen has been lodged in the collections of Museum Victoria, Melbourne, Victoria, Australia, registration number M53584. The probe block used for analysis has been registered as BM2016,2 and is stored in the types collection of the Natural History Museum, London, UK.

2. Occurrence, location and physical and optical properties

Hydroxyferroroméite was collected by Georges Favreau in April 2012 at the Correc d'en Llinassos ("Llinassos Brook" in Catalan), situated near the village of Oms in the Pyrénées-Orientales Department, France, some 15 km north of the Spanish border (42°32'16"N, 2°42'26"E). Only two specimens of the new mineral are known to exist. Correc d'en Llinassos is also the type locality for omsite (IMA2012–025), $Ni_2Fe^{3+}(OH)_6[Sb(OH)_6]$ (Mills *et al.*, 2012).

Hydroxyferroroméite occurs as yellow to yellow-brown powdery boxwork replacements up to about 50 μm across after tetrahedrite in a siderite–quartz matrix. The boxwork veins themselves are replaced by a more vitreous, yellow-brown form of hydroxyferroroméite (Figure 1). The type specimen is only 1 × 1 cm in dimension. The only other species associated on the type specimen are hematite, goethite, chalcopyrite, tetrahedrite and native

antimony. The tetrahedrite and chalcopyrite mineralization occurs within a siderite-rich vein capped by impermeable shale. A more detailed description of the deposit can be found in Berbain & Favreau (2007) and Mills *et al.* (2012). The mineral has formed from the decomposition of tetrahedrite, under mildly acidic and oxidising conditions.

Hydroxyferroroméite has a yellow streak and an earthy to vitreous lustre. The Mohs hardness is ~ 3 for fine-grained material, by analogy with other members of the roméite group, although large octahedra, if found, might be harder: well-crystallized hyroxycalcioroméite (Atencio *et al*., 2010), the former "lewisite" of Hussak and Prior (1895), has a hardness of 5½. Hydroxyferroroméite has a conchoidal fracture on the boxwork veins. No other physical properties could be determined because there are no crystals of the new mineral. Optical properties could not be measured due to the very fine-grained and porous nature of the material. The Gladstone-Dale compatibility index predicts n_{ave} = 1.898.

Hydroxyferroroméite also occurs at the Consols Mine (ABH Consols Mine; Australian Broken Hill Consols Mine), Broken Hill, New South Wales, Australia (Ian Graham, pers. comm.), where it occurs with chlorargyrite and dyscrasite (Australian Museum specimen D53310 and Museum Victoria specimen M50021).

3. Chemical composition

Nine quantitative chemical analyses were carried out on a fragment of hydroxyferroroméite by means of an electron microprobe (WDS mode, 15 kV, 10 nA and 1 μm beam diameter) at the Natural History Museum, London. The mineral is a member of the pyrochlore supergroup with general stoichiometry $A_2B_2X_6Y$, where A = non-framework cations (ideally 8-coordinated), B = octahedrally coordinated framework cations, X = framework anions and Y =

non-framework anions. A complication with this mineral is that the valence states of three cations, Fe, Cu and Sb, needed to be ascertained. The distribution of the cations between *A* and *B* sites depends on valence, since the more strongly bound Fe^{3+} and Sb^{5+} species are likely to occupy *B* sites while the larger, more weakly bound Fe^{2+} and particularly Sb^{3+}, with its stereoactive lone-pair electrons, are more likely to be in *A* sites (Atencio *et al*., 2010). Since *B* sites are likely to be fully occupied, while *A* sites may be partially vacant, the total number of cations per formula unit depends on valence determination, as does the amount of H needed for charge balance, and hence minimum H_2O content.

There are few techniques available that allow determination of valence for individual elements from small amounts of material. Mössbauer spectroscopy is frequently used for Fe (cf. Génin *et al*., 2014) and can be used for Sb (Friedl *et al*., 1992; Bayliss *et al*., 2010); X-ray near-edge absorption spectroscopy (XANES) can be used to determine valence, along with extended X-ray absorption fine structure (EXAFS) to ascertain coordination environment at a synchrotron for any of these elements (cf. Dilnesa *et al*., 2014 and Noël *et al*., 2014 for Fe; Mills *et al*., 2014, for Sb; Pekov *et al*., 2014 for Fe and Sb), if there is not interference from other elements in critical energy ranges. However, both Mössbauer and X-ray absorption spectroscopies require completely separate experimental setups for each element. This is not the case for X-ray photoelectron spectroscopy (XPS), which we elected to use for the present study. One of the few limitations of XPS is that since it involves irradiation of the sample with soft X-rays, it is a surface characterization technique, and may provide data on altered coatings rather than the bulk sample. XPS was used to determine the valence of Fe, Cu and Sb in hydroxyferroroméite powder as described below, and showed that Fe and Cu were in the +2 state while Sb was +5. The absence of Fe^{3+} suggests that the data reflects bulk valences rather than an oxidized surface film. Cations were allocated to *A* and *B* sites on the

basis of the valence data, *B* sites assumed to be fully occupied (2 *B pfu*), the number of oxygen atoms in the corresponding anhydrous formula calculated, and H_2O then calculated on the basis of 7 (O+OH+H_2O) *pfu*. Given the experimental impossibility of locating hydrogen atoms in the structure, the assumptions were made that (i) O^{2-} and H_2O in the *Y* site combined to form $2OH^-$ as far as possible, and (ii) *Y*-site oxygen atoms would be protonated fully before protonation of *X*-site oxygen atoms began, since protonation of *X* anions requires weaker bonding in the pyrochlore framework, while this is not the case for the non-framework *Y* anions. Thus, O_6 in *X* and (H_2O) in *Y* was preferred over (O_5(OH)) in *X* and (OH) in *Y*. This contrasts with the situation in the elsmoreite group of the pyrochlore supergroup, where substantial substitution of low-valent (Fe^{3+}, Al) for W^{6+} in the *B* sites lowers the mean *B*–*X* bond valence, and hence favours partial protonation of *X* anions (Mills *et al*., 2016a). The estimated content of H_2O based on the assumptions above was such that all *X* site anions were O^{2-}, while *Y* sites could contain (O, OH) or (OH, H_2O) in the formula thus calculated, although the Raman spectrum indicated that a small amount of H_2O was always present, presumably in the *Y* site. No other elements were detected. Analytical data are given in Table 1. The total is slightly low due to the porosity of the hydroxyferroroméite powdery masses.

The empirical formula (based on 7 (O + OH) *pfu*) for hydroxyferroroméite is: $(Fe^{2+}_{1.07}Cu^{2+}_{0.50}Zn_{0.03}Sr_{0.03}Ca_{0.01}\square_{0.36})_{\Sigma 2}(Sb^{5+}_{1.88}Si_{0.09}Al_{0.02}As_{0.01})_{\Sigma 2}O_6((OH)_{0.86}O_{0.14})$. The name corresponds to predominance of Fe^{2+} among the divalent cations that are dominant in the *A* sites, Sb^{5+} in *B* and OH^- in *Y*. If *Y* is OH-dominant and *B* is entirely Sb, then charge balance requires that the total charge in the *A* sites is close to +3, so these cannot be fully occupied by divalent cations such as Fe^{2+}. For simplicity and reproducibility, the pyrochlore-supergroup nomenclature scheme of Atencio *et al*. (2010) bases names upon the preponderant species of preponderant

valence group in each site of the structure. However, the variety of possible coupled substitutions is such that a valid species name to be associated with either one, several or no end-members in the sense of Hawthorne (2002). Fortunately, the name hydroxyferroroméite corresponds to only the end-member $(Fe^{2+}_{1.5}\square_{0.5})Sb^{5+}_2O_6(OH)$, which is therefore the simplified ideal formula of the mineral. Other end-members of the types $(Fe^{2+}A^{1+})Sb^{5+}_2O_6(OH)$ or $Fe^{2+}_2(Sb^{5+}B^{4+})O_6(OH)$ lie at the boundaries of the composition field with other, hypothetical, species; the analysis shows that there is little substitution towards either of these in type hydroxyferroroméite. The simplified formula requires FeO 24.48, Sb_2O_5 73.48 and H_2O 2.05, total 100 wt%.

4. Spectroscopy

X-ray Photoelectron Spectroscopy (XPS) data were acquired using a Kratos Axis ULTRA X-ray Photoelectron Spectrometer incorporating a 165 mm hemispherical electron energy analyser. The incident radiation was monochromatic Al *K*α X-rays (1486.6 eV) at 150 W (15 kV and 10 mA). Survey (wide) scans were taken at an analyser pass energy of 160 eV, and multiplex (narrow) high resolution scans at 20 eV. The scanned area was about 0.8 × 0.3 mm and the penetration depth less than 10 nm. Survey scans were carried out over the 1200–0 eV binding energy range, with 1.0 eV steps and a dwell time of 100 ms. Narrow high-resolution scans were run with 0.05 eV steps and 250 ms dwell time. Base pressure in the analysis chamber was 1.0×10^{-9} torr, and pressure during sample analysis was 1.0×10^{-8} torr. The XPS spectra showed the presence of only Fe^{2+}, Cu^{2+} and Sb^{5+} in the sample, with no Fe^{3+}, Cu^{1+} or Sb^{3+} (Figure 3). Minor Sb^0 is interpreted as due to the presence of native antimony in the boxwork.

Raman spectra were obtained using a micro/macro Jobin Yvon LabRam HRVIS, equipped with a motorized x-y stage and an Olympus microscope. The backscattered Raman signal was collected with a 20× objective and the Raman spectrum was obtained for a non-oriented single crystal. The 532 nm line of a He–Ne laser was used as excitation; laser power (80 mW) was controlled by means of a series of density filters. The minimum lateral and depth resolution was set to a few μm. The system was calibrated before each experimental session using the 520.6 cm^{-1} Raman band of silicon. The spectra were collected with multiple acquisitions (2 to 4), with single counting times ranging between 50 and 100 seconds. Spectral manipulation such as baseline adjustment, smoothing and normalization were performed using the *Labspec 5* software package (Horiba Jobin Yvon, 2004, 2005). After background removal, band component analysis was undertaken using the *Fityk* software package (Wojdyr, 2010), which enabled the type of fitting function to be selected and allows specific parameters to be fixed or varied accordingly.

The Raman spectrum (Figure 4) is characterized by a very intense band at 650 cm^{-1} (Sb–O bridging) with a medium shoulder at 709 cm^{-1} (Bahfenne *et al.*, 2011) and a very weak band at 568 cm^{-1}. In the region 300–600 cm^{-1}, multiple Raman bands are observed at 358, 436, 466 cm^{-1} (Sb–O vibrations), while bands lower than 300 cm^{-1} (180 and 271 cm^{-1}) correspond to lattice modes (Bahfenne *et al.*, 2011). In the region of 1000–4000 cm^{-1}, the spectrum displays bands at 1608, 1706 and 1773 cm^{-1}, which can be described as H–O–H bending modes, while bands at 2936, 3074 and 3634 cm^{-1} are assigned to OH stretching modes. The presence of H–O–H bending modes indicates that a small proportion of the OH is replaced by $O + H_2O$ in the *Y* site.

5. X-ray diffraction and crystallography

X-ray powder diffraction data were obtained with a Phillips X'Pert Pro PW3040 powder diffractometer using Cu*K*α radiation at Museum Victoria. Data (*d* spacings in Å) are given in Table 2. The unit cell parameters refined from the powder data are: Space group: *Fd*-3*m*, *a* = 10.251(31) Å, *V* = 1077(6) Å^3 and *Z* = 8. The poorly crystalline nature and small number of peaks in the powder pattern (7) contributed to the larger than usual error in the unit cell parameters.

Although it was not possible to refine the structure, the high symmetry and location of atoms on special positions allow some deductions to be made about the details. The pyrochlore structure has site coordinates *A* = 16*c* [0; 0; 0], *B* = 16*d* [½; ½; ½], *X* = 48*f* [*x*; ⅛; ⅛] and *Y* = 8*b* [⅜;⅜;⅜]. The shortest *B*···*B* site distance is thus $^1/_{\sqrt{8}}a$ = 3.624 Å. If the *B* site is completely occupied by Sb^{5+}, then *B*–*X* bonds have a bond valence of $^5/_6$ and the Sb^{5+}–O parameterization of Mills *et al*. (2009) implies a bond distance of 1.924 Å. The free coordinate of the *X* site is then estimated as *x* = 0.3131 accordingly. The *A*–O bond distances are then *A*–*X* = 6 × 2.637 Å and *A*–*Y* = 2 × 2.219 Å. Note that 75% occupation of the *A* site by Fe^{2+} is compatible with the *Y* oxygen atom having three Fe neighbours rather than four, while the hydroxyl H atom completing the coordination tetrahedron around oxygen. This suggests strongly that there is short-range ordering of Fe and H atoms and *A*-site vacancies. The model average structure is depicted in Fig. 5.

If the *A* site is 75% occupied by Fe^{2+}, the bond-valence parameters of Brese and O'Keeffe (1991) imply that the respective bond valences are *A*–*X* = 0.087 *v.u.* and *A*–*Y* = 0.270 *v.u*., while bond-valence sums are: *A* = 1.062 *v.u.* as opposed to the expected 2.0 *v.u*, *X* = 1.797 *v.u.* (including Sb–O bonds) and *Y* = 0.808 *v.u*. Thus, if Fe is situated at the ideal *A* site, then Fe is strongly underbonded, and all anions are slightly so.

In accord with the Distortion Theorem (cf. Brown, 2009), the bond-valence sum on Fe can be increased if the Fe atom is displaced away from the ideal *A*-site position. The size of displacement required to achieve a bond-valence sum of 2.0 *v.u.* varies as a function of direction. Since the *A* site has point symmetry -32*m*, the full sphere of directions around it can be decomposed into twelve equivalent triangles of the type seen in Fig. 6a, bounded by the directions [111], [-111] and [-1-11]. These directions are position vectors for the corners of a 45° right-angled triangle that is half of one of the faces of a cube. For the *A* atom at [½;½;½], ±[111] vectors point towards *Y* atoms, respectively labelled as *Y*1 and *Y*2 in Fig. 6, while *A*–*X* vectors are nearly but not exactly parallel to the other <111> directions. Figure 6b shows a contour plot of the displacement magnitude at which Fe bond valence becomes 2.0 *v.u.* or as close as possible to that value, as a function of direction within this triangle. The minimum displacement of 0.63 Å occurs if Fe is moved directly towards a *Y* atom, but takes values close to 1.0 Å over much of the triangle. For directions very close to <100>, even larger displacements are needed, or a maximum possible bond valence of less than 2.0 *v.u.* is the maximum attainable.

The large displacements required, and the need to avoid very close approaches to *X* atoms, imply that the Fe displacement direction is unlikely to be more than about 45° from the *Y*1–*A*–*Y*2 axis (blue and green zones in Fig. 6b). Fe–*Y* bond valences are strongly affected by the displacement, and the directions favourable for Fe to displace also result in strong overbonding for hydroxide oxygen atom *Y*1 (> 1.0 *v.u.* bond valence, compared with the ideal value of 0.33 *v.u.*: Fig. 6c) and underbonding for *Y*2 (<0.1 *v.u.*: Fig 6d). The very weak Fe⋯*Y*2 bonding suggests that Fe coordination is better regarded as 6+1 rather than 6+2. However, overbonding of *Y*1 can only be compensated by movement of the *Y* oxygen atom

away from its nearby Fe atoms, with direction and magnitude depending on which Fe atoms are displaced towards or away from it (Fig. 6e and f). In conclusion, bond valence sums can be satisfied, despite Fe^{2+} being a rather small cation to occupy the *A* site of the pyrochlore structure, but this requires partial occupancy of *A* sites, short-range order, and coupled displacements of Fe from ideal *A* positions and of OH from *Y* positions. This study provides evidence that the relatively small divalent cation Fe^{2+} can substantially occupy the *A* sites of the pyrochlore structure, albeit with some local modification of the structure. This is in contrast to the situation recently found for "partzite", which was believed to be $Cu_2Sb_2O_7$ with the pyrochlore structure, containing the smaller divalent cation Cu^{2+}. Examination of type "partzite" showed it to consist of a nanoscale intergrowth of a Pb-dominant roméite-group phase, an amorphous Cu silicate and other minerals, with negligible Cu accommodated in the "plumboroméite" (Mills *et al*., 2016b). Thus, "partzite" has been discredited, and there remains no compelling evidence for "cuproroméite" minerals, consistent with the observation that the hydroxyferroroméite of this study has only about 30% of its ideal Fe^{2+} content replaced by Cu^{2+}, despite being derived from the Cu-rich primary mineral tetrahedrite.

Acknowledgements

We thank Alex Duan (Surface & Chemical Analysis Network, School of Chemistry, University of Melbourne) for help with obtaining the XPS results. Pierre Clolus is also thanked for taking the image of the type specimen.

References

Atencio D., Andrade M.B., Christy A.G., Gieré R., Kartashov P.M. (2010): The pyrochlore supergroup of minerals: nomenclature. *Can. Mineral.*, **48**, 673–698.

Bayliss, R., Berry, F.J., Bowden, A., Greaves, C., Thomas, M.F. (2010): Mössbauer spectroscopic study of some iron and antimony-containing minerals. *J. Physics: Conference Series*, **217**, #012049.

Berbain, C. & Favreau, G. (2007) : Un exemple peu courant de minéralisation nickélifère: le Correc d'en Llinassos à Oms (Pyrénées-Orientales). *Le Cahier des Micromonteurs*, **95**, 3–24.

Brese, N.E. & O'Keeffe, M. (1991): Bond-valence parameters for solids. *Acta. Cryst*., **B47**, 192–197.

Brown, I.D. (2009): Recent developments in the methods and applications of the bond valence model. *Chem. Rev*., **109**, 6858–6919.

Christy, A.G. & Atencio, D. (2013): Clarification of status of species in the pyrochlore supergroup. *Mineral. Mag.*, **77**, 13–20.

Dilnesa, B.Z., Wieland, E., Lothenbach, B., Dähn, R., Scrivener, K.L. (2014): Fe-containing phases in hydrated cements. *Cement and Concrete Research*, **58**, 45–55.

Friedl, J., Wagner, F.E., Sawicki, J.A., Harris, D.C., Mandarino, J.A., Marion, Ph. (1992): ^{197}Au, ^{57}Fe and ^{121}Sb Mössbauer study of gold minerals and ores. *Hyperfine Interactions*, **70**, 945–948.

Génin, J.-M.R., Mills, S.J., Christy, A.G., Guérin, O., Herbillon, A.J., Kuzmann, E., Morin, G., Ona-Nguema, G., Ruby, C., Upadhyay, C. (2014): Mössbauerite, $Fe^{3+}_6O_4(OH)_8CO_3{\cdot}3H_2O$, the first fully oxidised "green rust" mineral, from Mont Saint-Michel Bay, France. *Mineral. Mag*., **78**, 447-465.

Hawthorne, F.C. (2002): The use of end-member charge-arrangements in defining new mineral species and heterovalent substitutions in complex minerals. *Can. Mineral*., **40**, 699–710.

Hussak, E. & Prior, G.T. (1895): Lewisite and zirkelite, two new Brazilian minerals. *Mineral. Mag*., **11**, 80–88.

Mills, S.J., Christy, A.G., Chen, E.C.-C., Raudsepp, M. (2009): Revised values of the bond valence parameters for $^{[6]}$Sb(V)–O and $^{[3–11]}$Sb(III)–O. *Zeitschr. Kristallogr.*, **224**, 423–431.

Mills, S. J., Kampf, A. R., Housely, R. M., Favreau, G., Pasero, M., Biagioni, C., Merlino, S., Berbain, C., Orlandi, P. (2012): Omsite, $(Ni,Cu)_2Fe^{3+}(OH)_6[Sb(OH)_6]$, a new member of the cualstibite group from Oms, France. *Mineral. Mag.*, **76**, 1347–1354.

Mills, S.J., Etschmann, B., Kampf, A.R., Poirier, G., Newville, M. (2014): Sb^{5+} and Sb^{3+} substitution in segnitite: a new sink for As and Sb in the environment and implications for acid mine drainage. *Amer. Mineral.*, **99**, 1355–1359.

Mills, S.J., Christy, A.G., Rumsey, M.S., Spratt, J.G. (2016a): The crystal chemistry of elsmoreite from the Hemerdon (Drakelands) mine, UK: hydrokenoelsmoreite-3*C* and hydrokenoelsmoreite-6*R*. *Mineral.Mag.*, **80**, doi: 10.1180/minmag.2016.080.058.

Mills, S.J., Christy, A.G., Rumsey, M.S., Spratt, J. (2016b): Discreditation of partzite. *Eur. J. Mineral.*, **28**, (in press).

Noël, V., Marchand, C., Juillot, F., Ona-Nguema, G., Viollier, E., Marakovic, G., Olivi, L., Delbes, L., Gelebart, F., Morin, G. (2014): EXAFS analysis of iron cycling in mangrove sediments downstream a lateritized ultramafic watershed (Vavouto Bay, New Caledonia). *Geochim. Cosmochim. Acta*, **136**, 211–228.

Pekov, I.V., Zubkova, N.V., Göttlicher, J., Yapaskurt, V.O., Chukanov, N.V., Lukova, I.S., Belakovskiy, D.I., Jensen, M.C., Leising, J.F., Nikischer, A.J., Pushcharovsky, D.Y. (2014): Whitecapsite, a new hydrous iron and trivalent antimony arsenate mineral from the White Caps mine, Nevada, USA. *Eur. J. Mineral.*, **26**, 577–587.

Table 1. Analytical data for hydroxyferroroméite.

Constituent	wt%	Range	SD	Probe Standard
Sb_2O_5	67.10	64.72–70.43	1.63	Sb metal
As_2O_5	0.15	0.07–0.28	0.07	GaAs
SiO_2	1.17	0.65–2.02	0.44	wollastonite
Al_2O_3	0.28	0–1.94	0.65	corundum
CaO	0.18	0–1.40	0.46	wollastonite
SrO	0.58	0.47–0.77	0.11	celestine
FeO	16.95	15.60–17.66	0.72	fayalite
CuO	8.69	7.53–9.34	0.62	Cu metal
ZnO	0.54	0.40–0.72	0.11	Zn metal
H_2O_{calc}	1.72	1.15–2.27	0.38	
Total	97.36	96.41–98.97	0.85	

Table 2. X-ray powder diffraction data for hydroxyferroroméite.

hkl	d_{obs}	d_{calc}	I/I_o
111	5.971	5.974	65
311	3.190	3.194	63
222	**3.069**	**3.067**	**100**
400	2.681	2.689	48
511	2.005	2.004	63
440	1.935	1.936	25
531	1.785	1.784	43

Figure 1. Georges Favreau at the outcrop at Correc d'en Llinassos. The massive siderite (dark brown) is at the bottom of the mineralization, with shale (yellow) capping the mineralization.

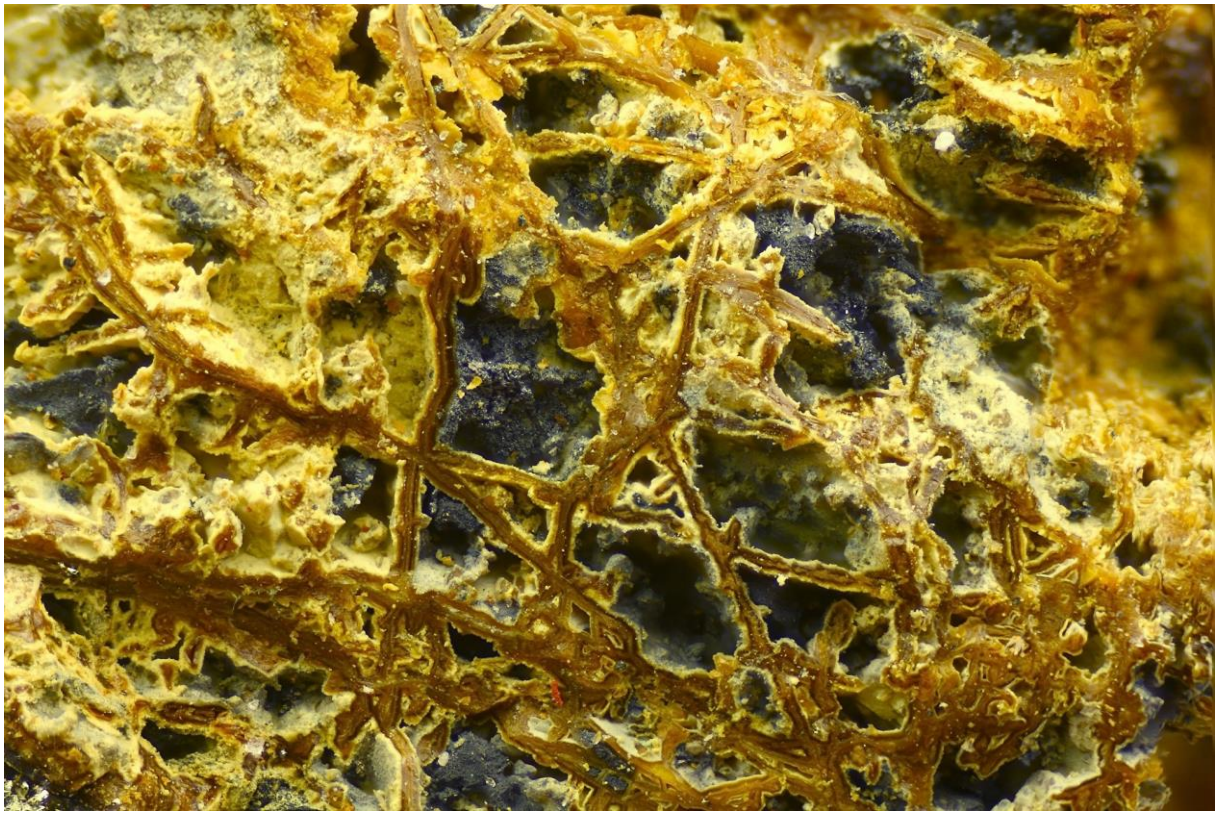

Figure 2. Hydroxyferroroméite powder and boxwork with tetrahedrite and antimony. FOV 2.8 mm across. Specimen Georges Favreau, photo Pierre Clolus.

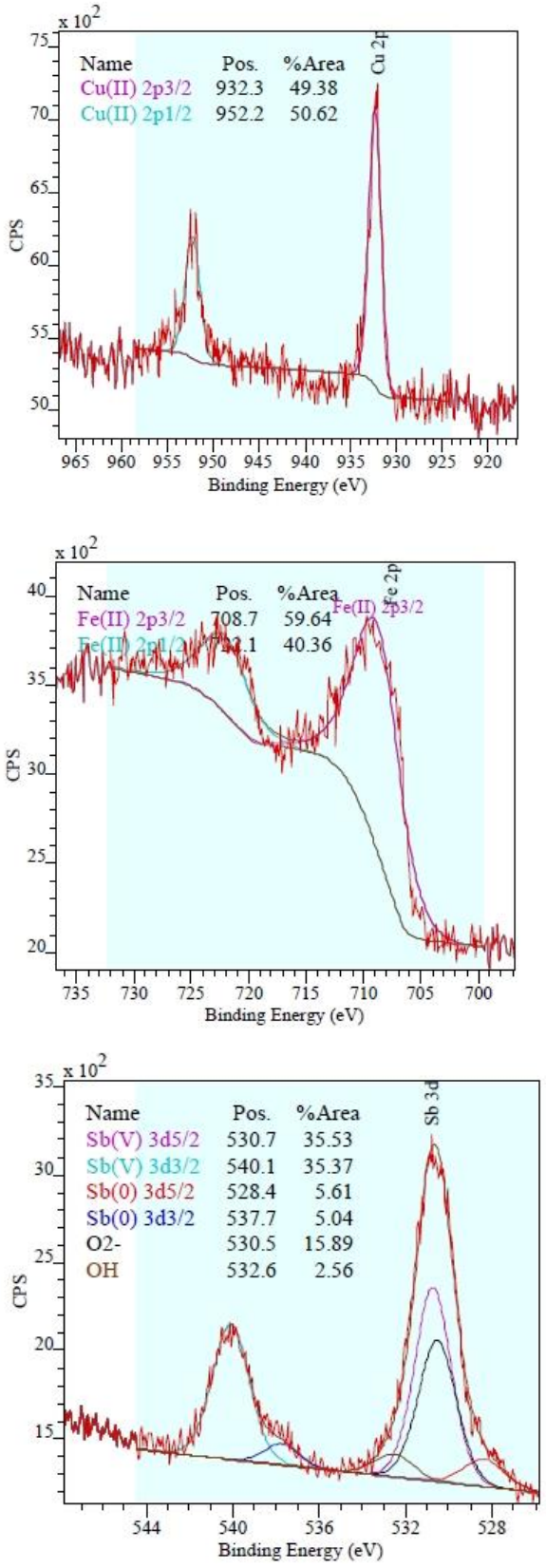

Figure 3. XPS spectra of hydroxyferroroméite for Cu, Fe and Sb.

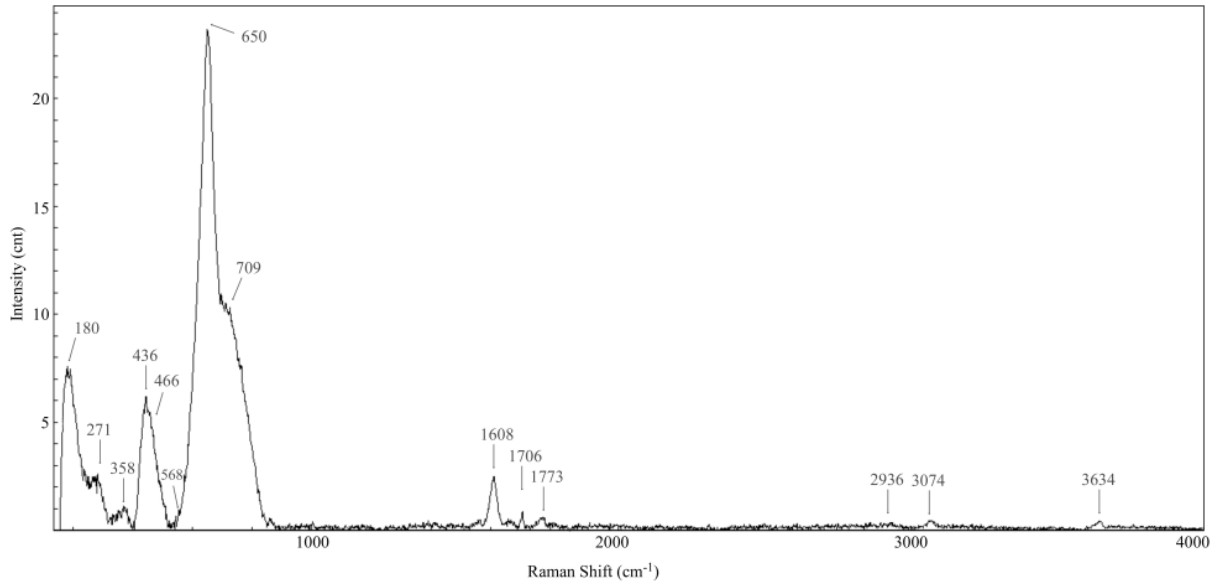

Figure 4. Raman spectra of hydroxyferroroméite collected over the 170–4000 cm^{-1} range.

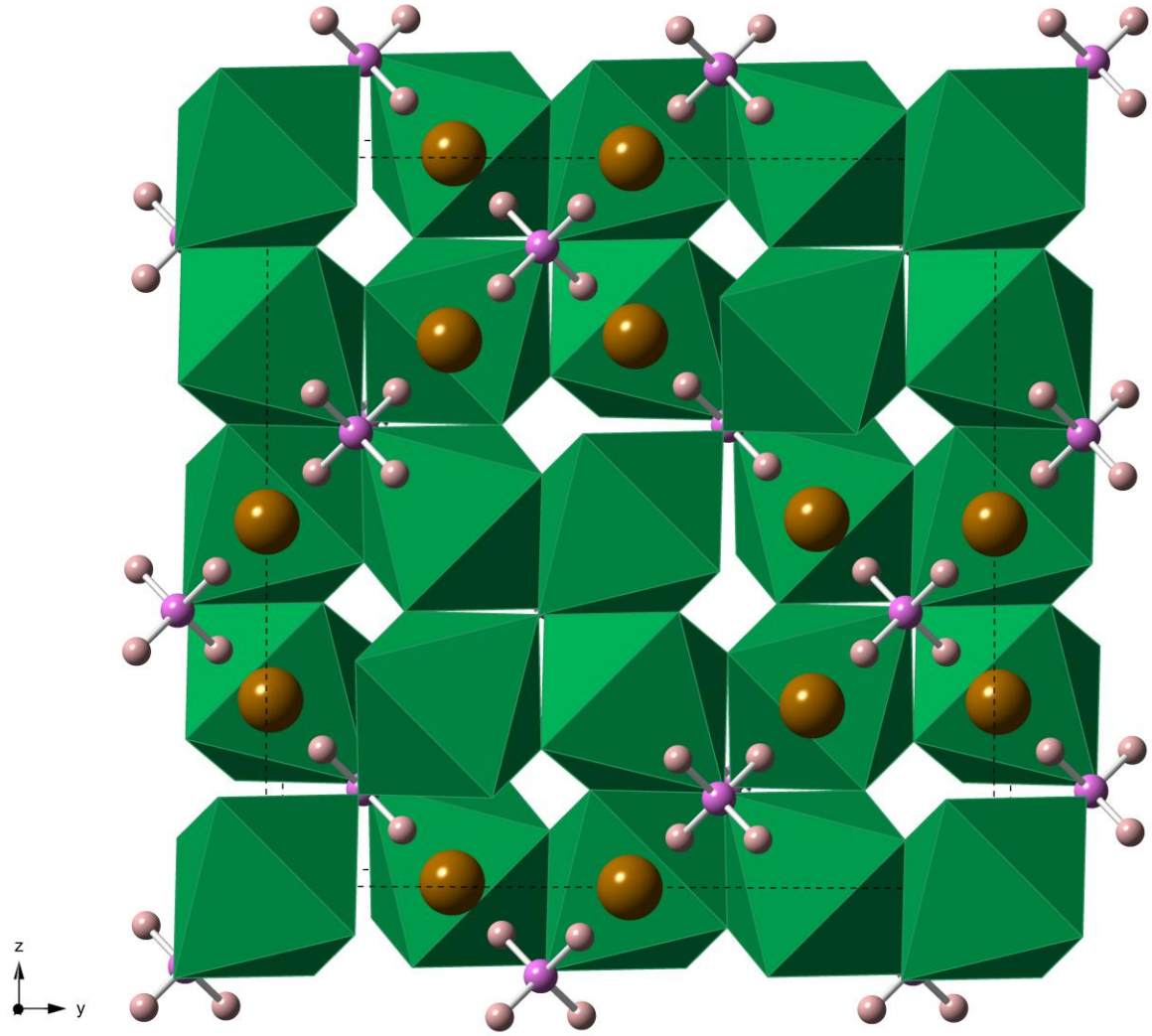

Figure 5. Model average structure for hydroxyferroroméite, derived as described in the text and viewed nearly down the **x** direction. SbO_6 octahedra (green) share corners to form a typical pyrochlore-type B_2X_6 framework. *A* sites are 75% occupied by Fe^{2+} (brown spheres), which are necessarily displaced from the ideal position (see text), *Y* sites are fully occupied by oxygen (larger pink spheres), bonded to H atoms that are distributed over partially occupied sites (small pale pink spheres): the picture shows fourfold disorder of H positions. Short-range order would ensure that locally, each *Y*-site oxygen atom would be bonded to one H atom and three Fe atoms in an approximately tetrahedral configuration.

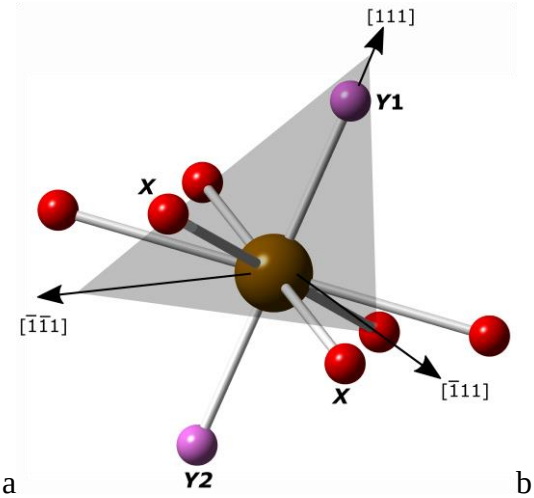
[111]
Y1
X
[$\bar{1}\bar{1}$1]
[$\bar{1}$11]
X
Y2

a

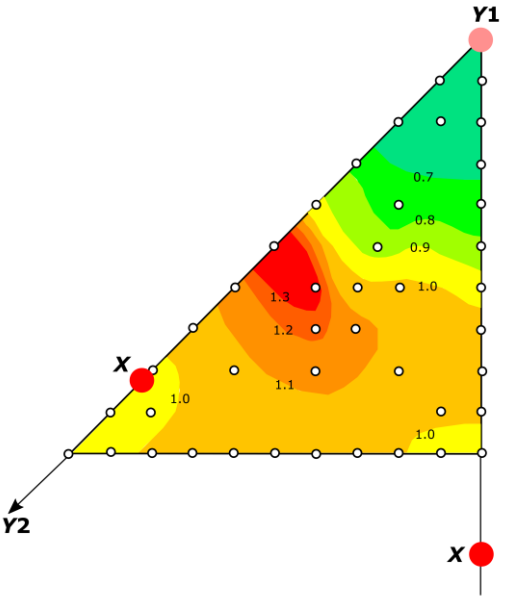
Y1
0.7
0.8
0.9
1.0
1.3
1.2
1.1
X
1.0
1.0
Y2
X

b

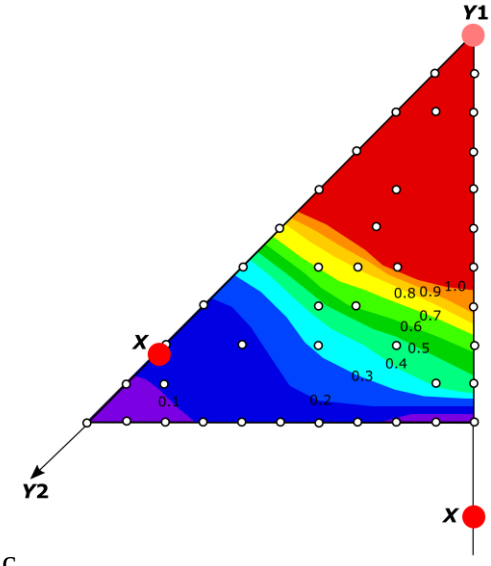
Y1
0.8
0.9
1.0
0.7
0.6
0.5
0.4
0.3
X
0.1
0.2
Y2
X

c

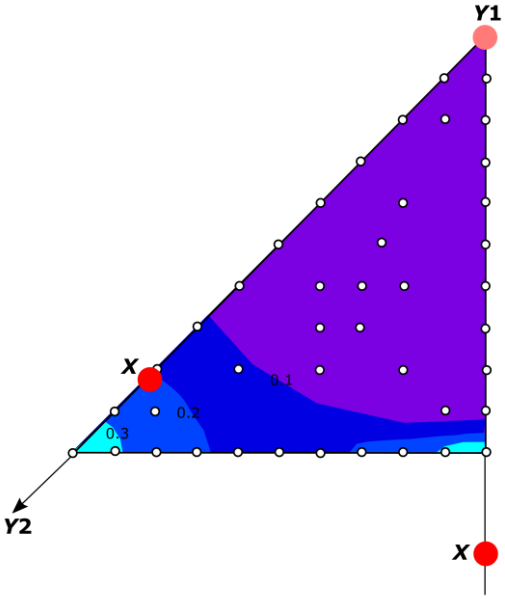
Y1
0.1
X
0.2
0.3
Y2
X

d

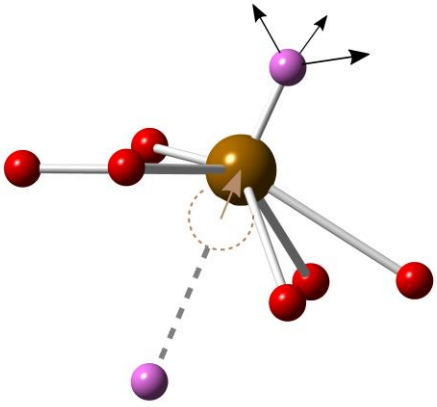

e

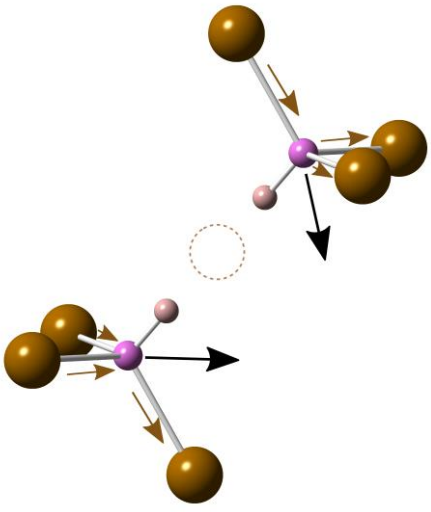

f

Figure 6. (a) Coordination around *A* site at [½; ½; ½] (brown sphere); six *X* ligands are shown as red spheres, two *Y* ligands as pink spheres. Grey triangle is plane onto which Fe displacement direction is projected gnomonically in parts b-d. (b) Contour map of distance in Å by which Fe must be displaced in each direction away from ideal *A* site in order to achieve a bond valence sum of 2.0 *v.u*. Small circles indicate calculation points. (c) Valence of bond from Fe to *Y*1 for the displacements of (b). (d) Valence of bond from Fe to *Y*2 for the displacements of (b). (e) Displacement of Fe atom (brown) increases bond-valence sum on Fe but reduces coordination number from 8 to 7; oxygen *Y*1 (upper pink sphere) must also move in order to avoid overbonding, but direction and magnitude of displacement depends on which out of three Fe neighbours move towards or away from it. (f) Two hydroxide groups (pink) with O–H bonds oriented towards one another along [111], across a vacant *A* site (dashed brown circle). Ideal O positions are 4.55 Å apart. Coordination tetrahedra completed by three Fe atoms (brown spheres) for both O atoms; Fe atoms may displace either towards or away from hydroxide oxygen atom (brown arrows), which in turn displaces in response to those movements (black arrows), so as to avoid overbonding.

Click here to download Figure UK CuFeSbO Oms FOV 2.8 mm coll GF photo PC-red.jpg

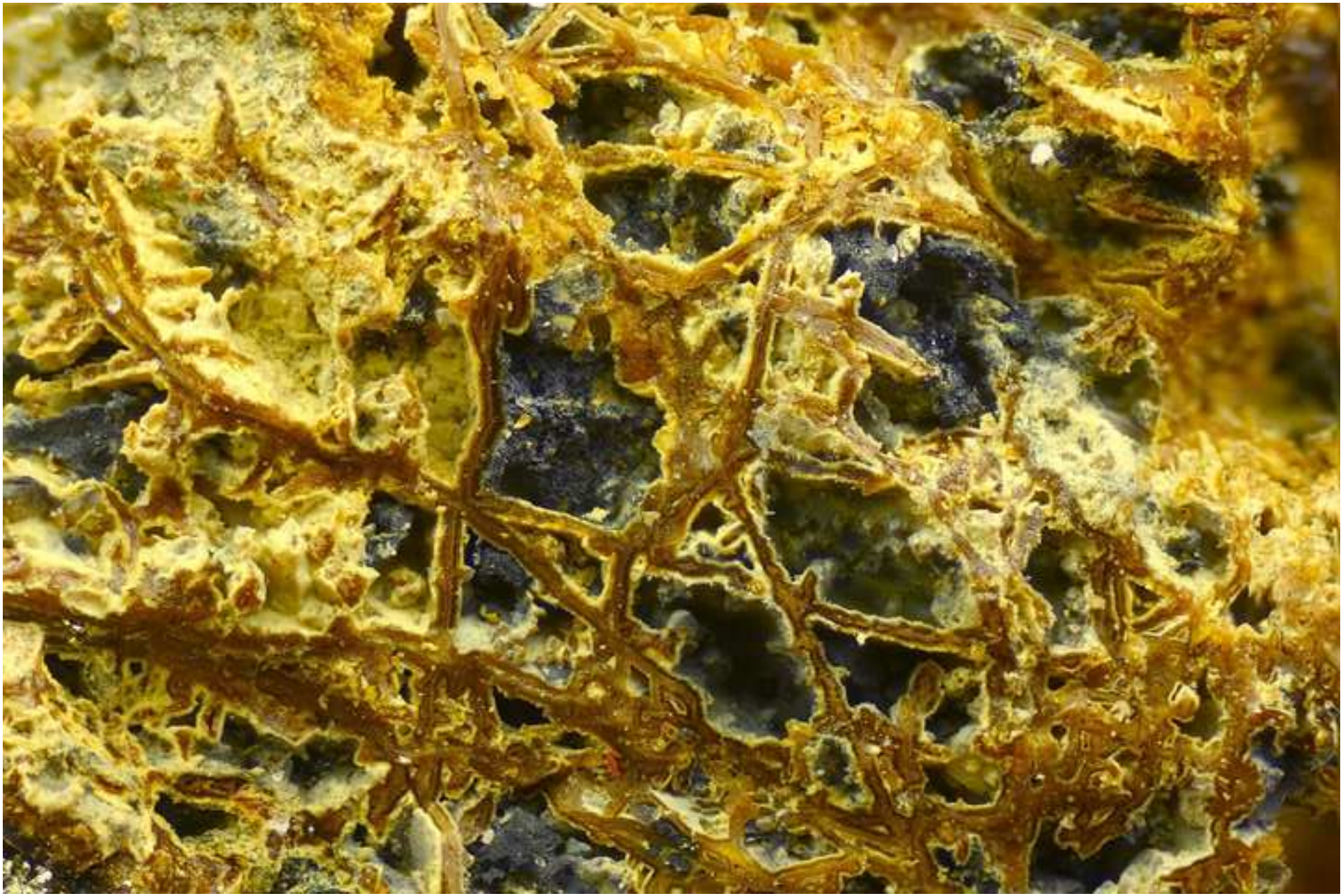

3a

Click here to download Figure cu xps.jpg

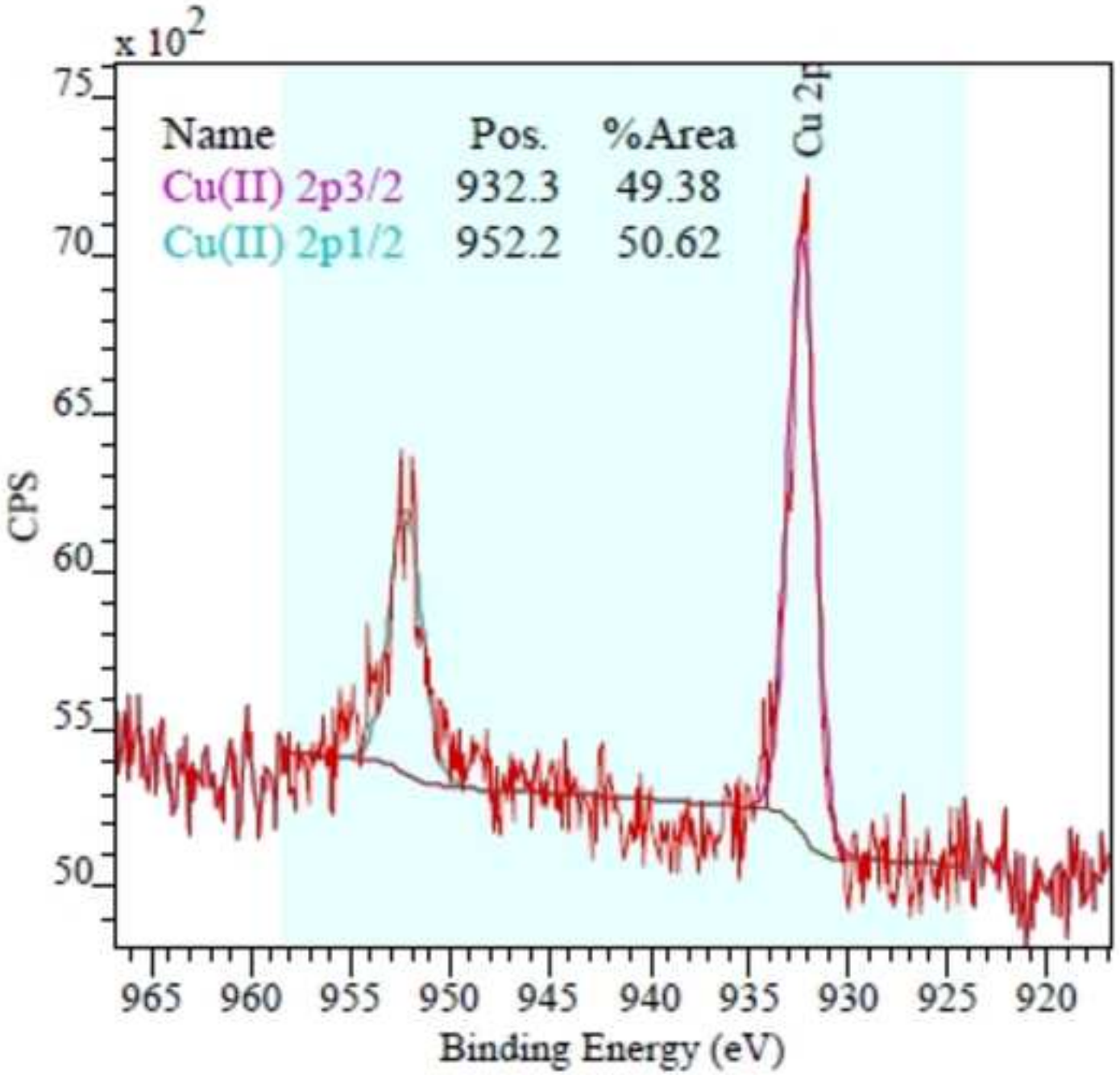

3b

Click here to download Figure fe xps.jpg

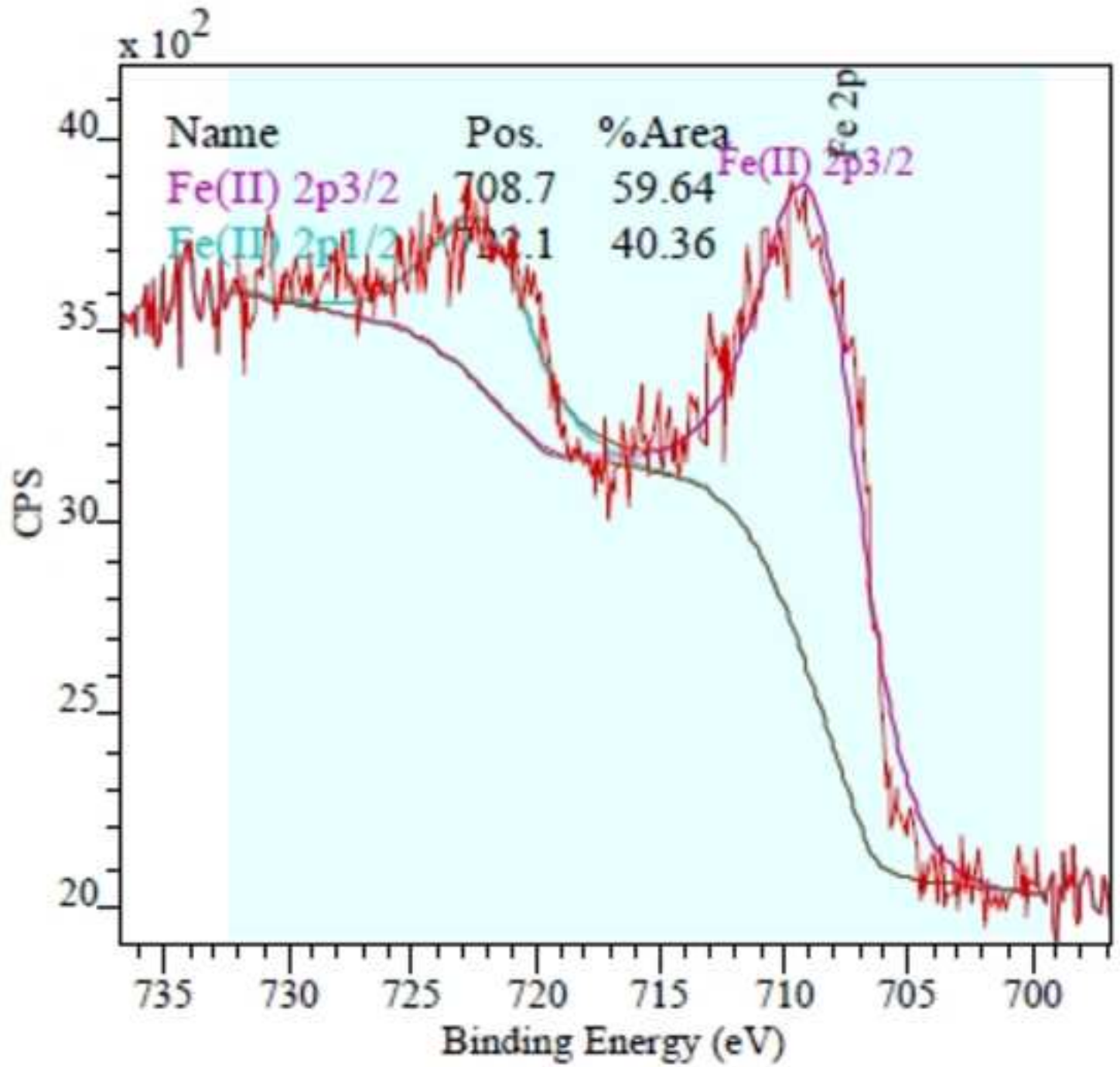

3c

Click here to download Figure sb xps.jpg

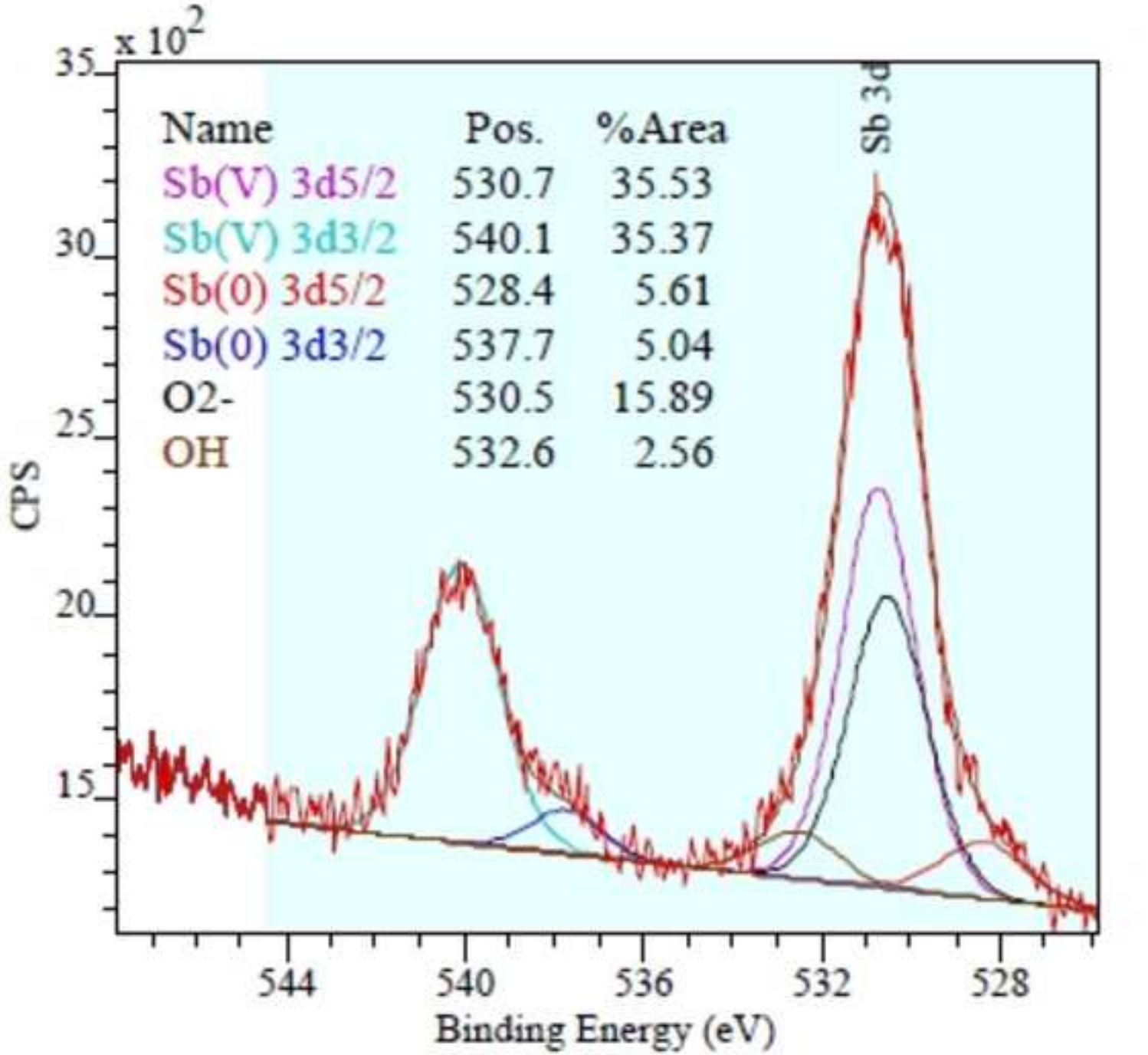

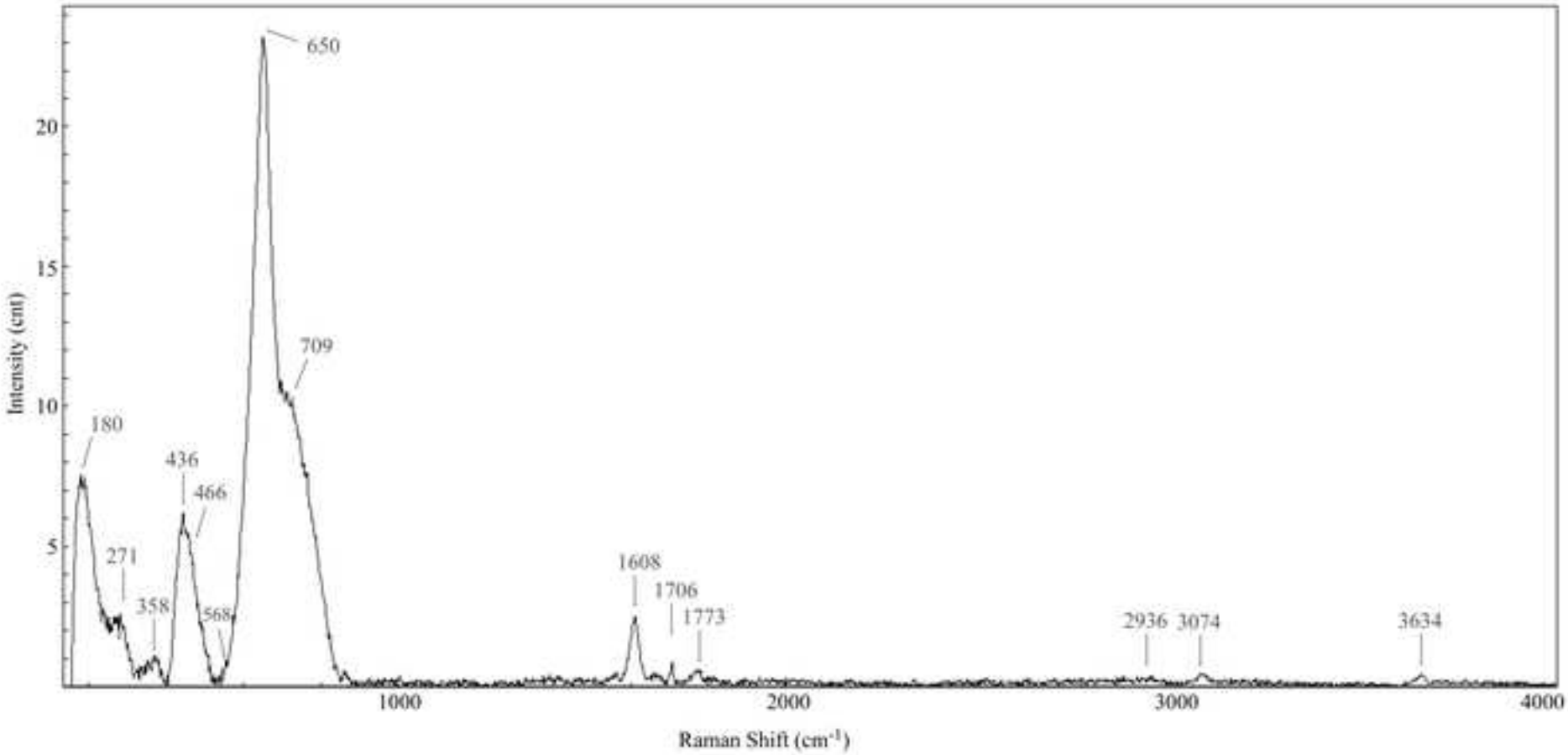

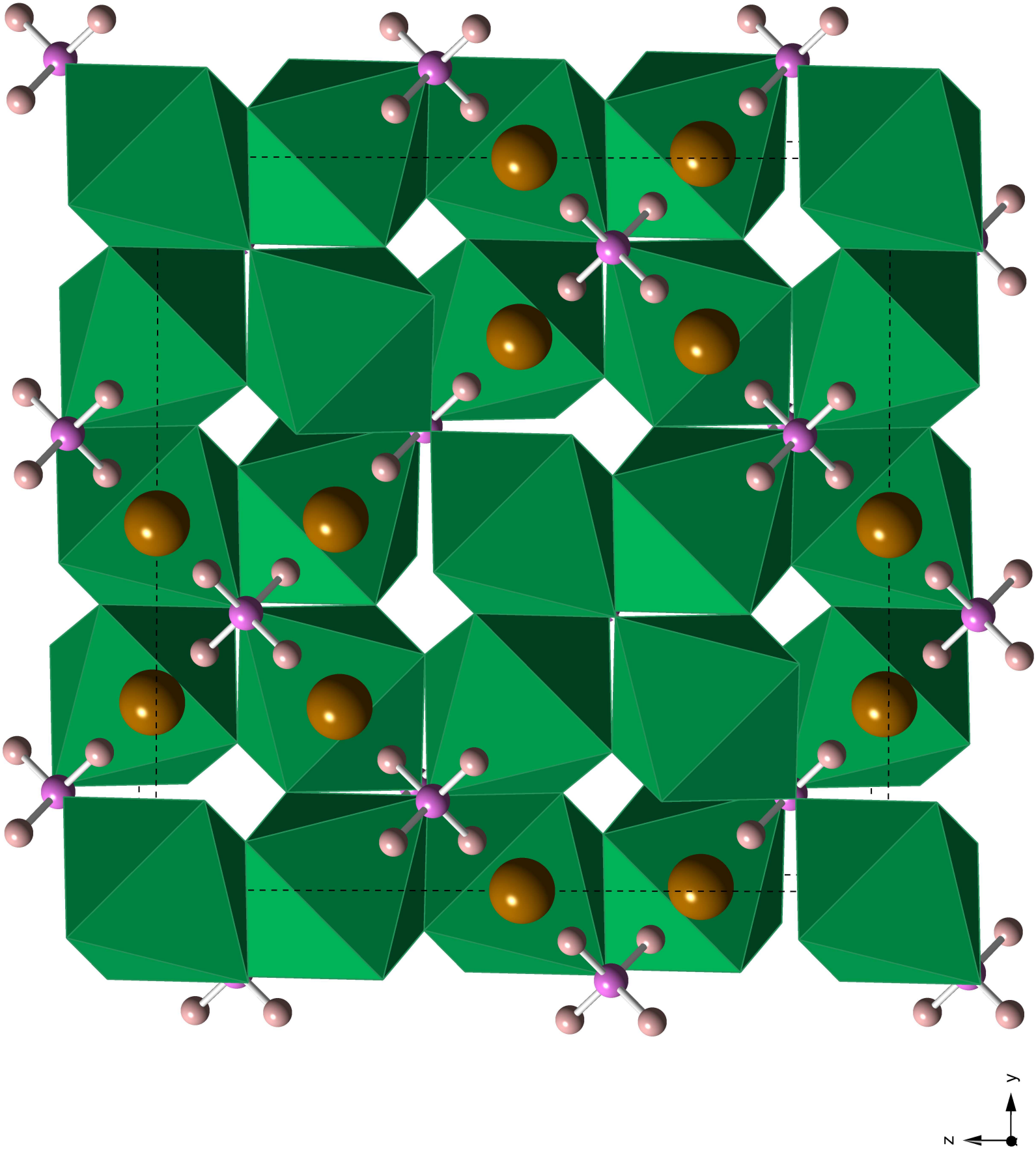
y
z

6a

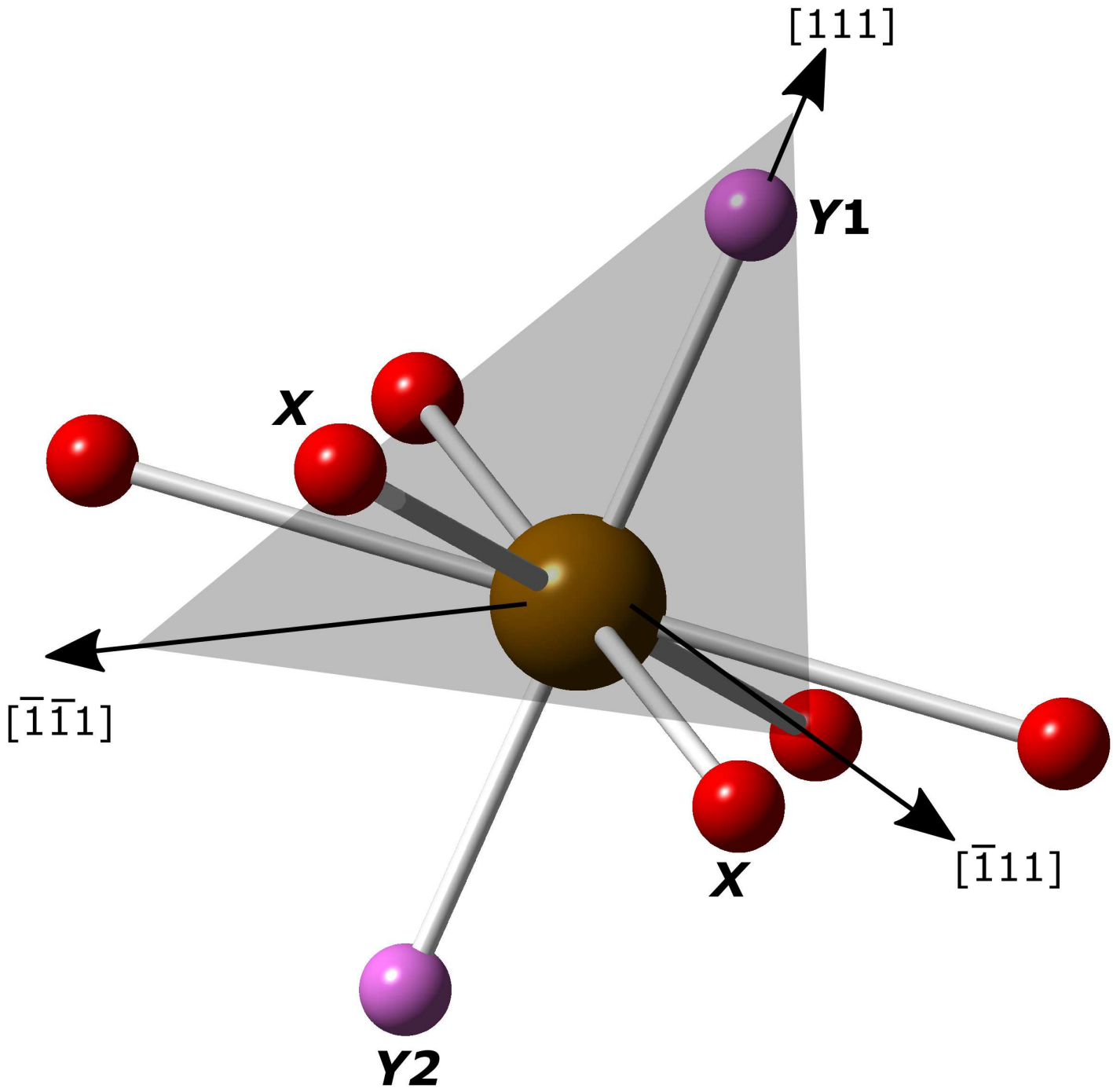

6b

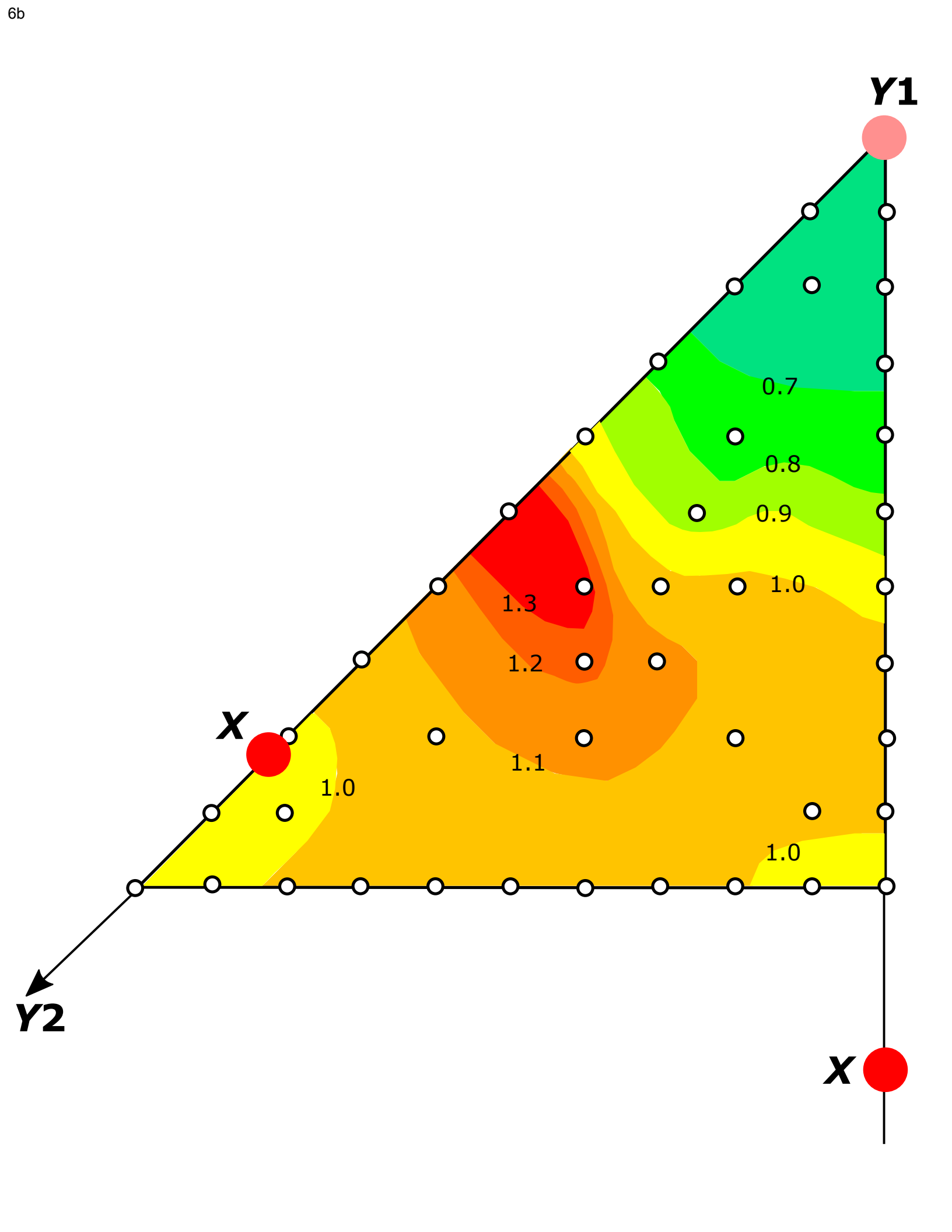

6c

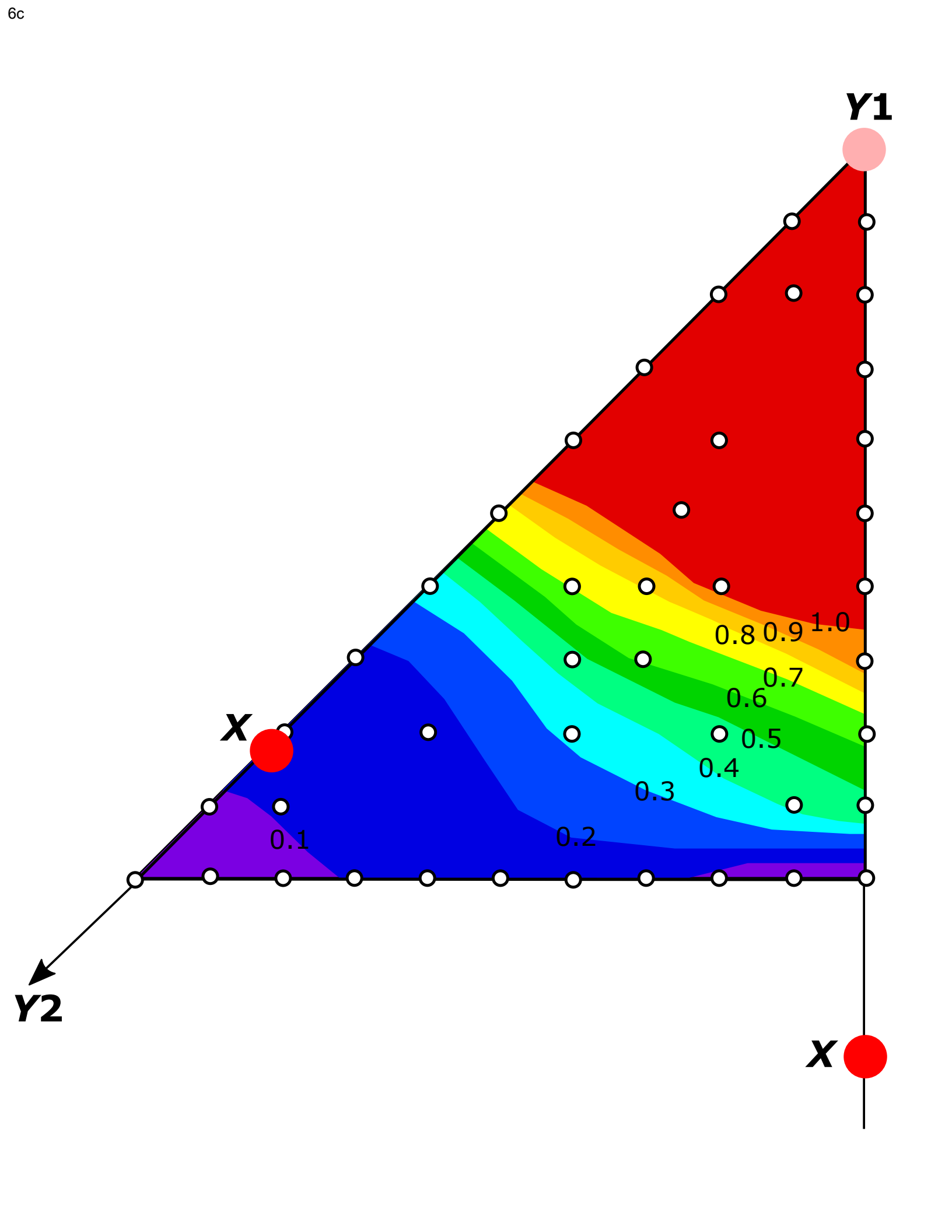

6d

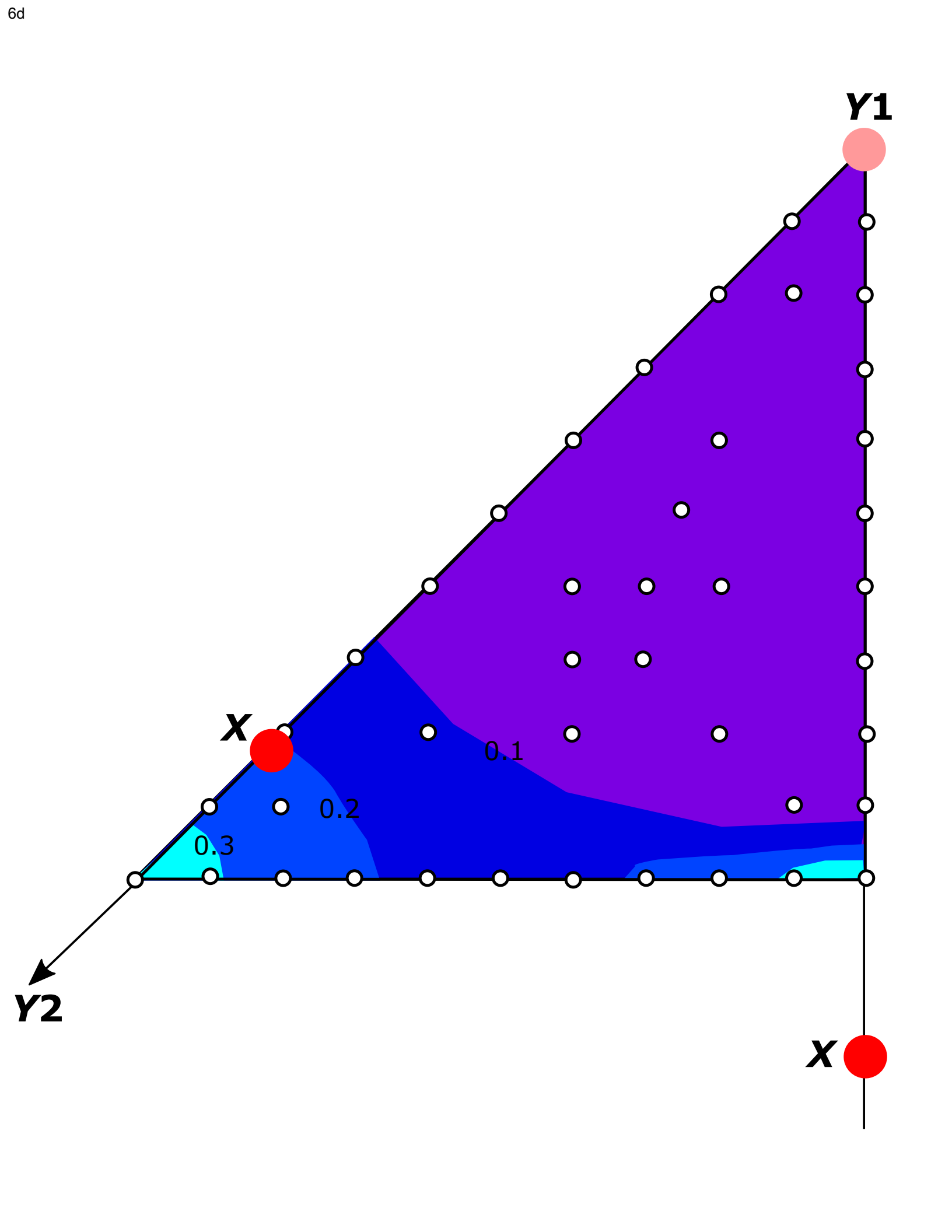

6e

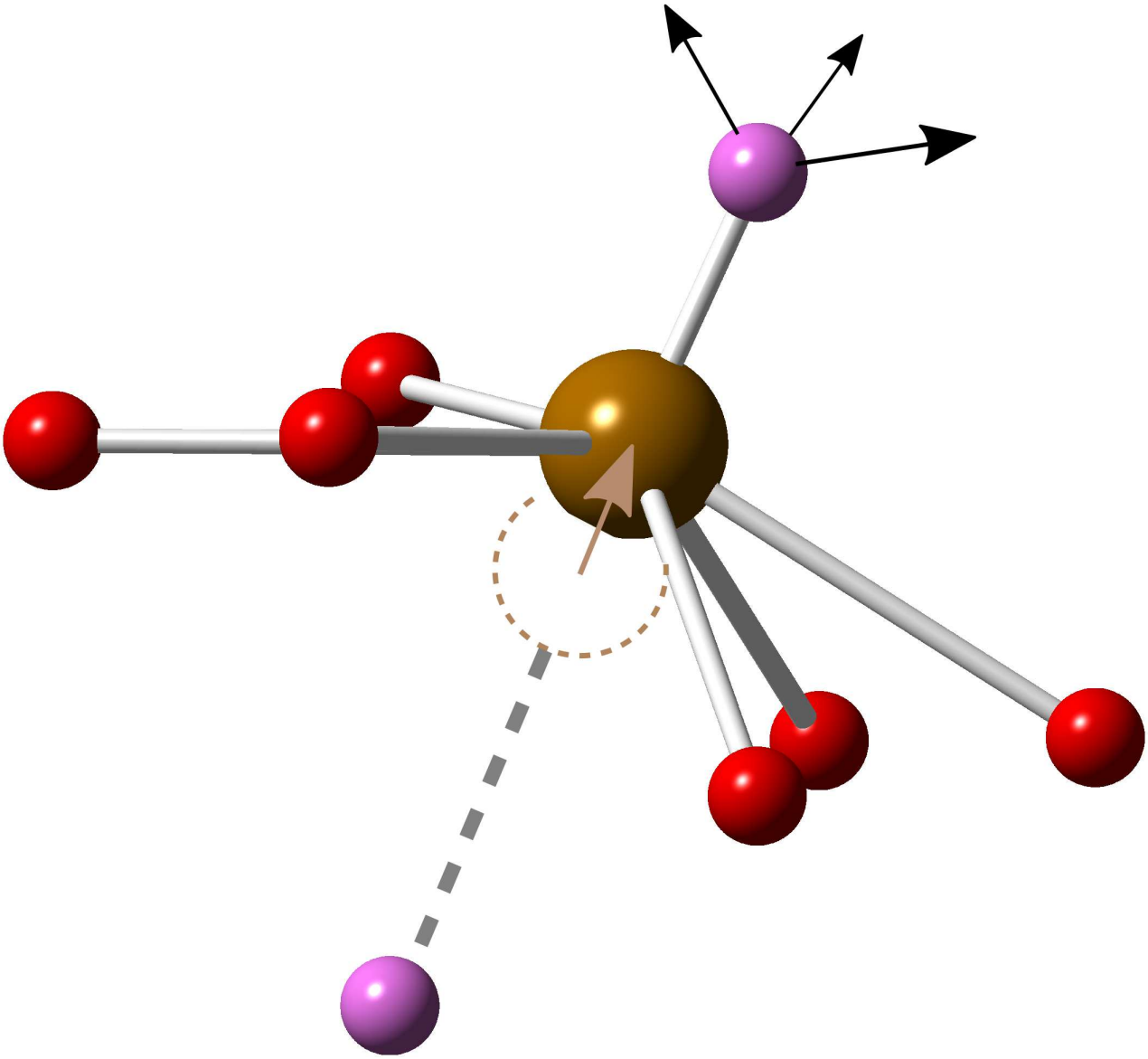

6f